TECHNICAL PAPER

Influence of the obstacles on dielectrophoresis-assisted separation in microfluidic devices for cancerous cells

Shayan Valijam[1] · Alireza Salehi[1]

Abstract

The development of a separation lab-on-a-chip device based on the particle size is critical in the early detection of circulating tumor cells. In this work, combining alternating current dielectrophoresis and drag force are used to precisely separate MDA-MB231 and red blood cells in the microfluidic platform. Four microfluidic devices with sidewall electrodes and different obstacle shapes were employed to both generate non-uniform fields inside the channels and condense the particles near the electrodes. Besides that, dividing the particles inlet into two main channels enable fast and accurate separation inside the device, and then particles deflected to the different outlets. Choosing the frequency is critical in the magnitude and sign of the dielectrophoresis force. Negative dielectrophoresis force was acting on both cancerous and red blood cells when the frequency was 10 kHz. Finite element simulation was conducted to predict the particle trajectories and revealed that the device with rectangular obstacles had the higher electric field non-uniformity when the voltage applied was set to 6 V and − 6 with the frequency of 10 kHz, Simulation represented 100% separation efficiency and purity for cancerous cells in the specific outlets. Decreasing the voltage from 6 V and − 6 V to 5 V and − 5 V could reduce the separation efficiency to 46%. The appropriate value of voltage (6 V, − 6 V) was applied to the electrodes resulting in the lower Joule heating and sufficient dielectrophoresis forces.

Keywords Particle separation · Dielectrophoresis · Obstacles · Circulating tumor cells

1 Introduction

Lab-on-a-chip (LOC) systems based on microfluidic platforms have attracted considerable attention in order to manipulate cells, in recent years [1, 2]. The significant advantages of microfluidic devices are portability, consumption of low sample, reduction of analysis time and cost [3, 4]. Trapping [5], sorting [6] and separation [7] are critical in diagnostic applications of LOC systems to distinguish circulating tumor cells (CTCs) for early detection of disease and find appropriate treatments [8]. CTCs are detached from a primary tumor into the body by blood circulation. CTCs are considered seeds for the growth of the tumors. Cell separation is a procedure that separates or isolates mixtures of complex particles from solution. Herein, an in-depth study of circulating tumor cells in blood is helpful to predict the overall progression of cancers [9]. Various methods are utilized for the separation of the particles at microscale such as mechanical [10], magnetic [11], acoustic [12], optical [13] and electrical methods [14]. Electrical methods are divided into electrophoresis (EP) [15] and dielectrophoresis (DEP) [16] to manipulate the studied particles. Dielectrophoresis (DEP) is the phenomenon occurring owing to the interaction between a dielectric particle and a non-uniform electric [17, 18]. Inhomogeneous field is generated by using either direct current (DC) [19] or alternating current (AC) field [20, 21] are called DC-DEP and AC-DEP, respectively. The microfluidic devices that are based on DC-DEP need high voltage to produce sufficient DEP force which leads to Joule heating effect inside the channel and damaging the particles. Gas bubble formation and increasing the temperature are due to Joule heating in the device [22]. The

✉ Shayan Valijam
shayanvalijam@email.kntu.ac.ir

Alireza Salehi
salehi@kntu.ac.ir

1 Faculty of Electrical Engineering, K. N. Toosi University of Technology, 1631714191 Tehran, Iran

AC-DEP separation devices, however, require low voltage and do not increase the channel temperature. It should be noted that Particle size, the dielectric properties of the particles and aqueous solution are important parameter in determining the type of the DEP force. The particles move toward the higher electric field regions in positive DEP, although in negative DEP the particles repel from the higher electric field regions and move toward the lower electric field regions. DEP is popular rather than other separation methods because of label-free nature, high purity, high separation efficiency and do not require any modification of sample like separation based on adhesion properties of the particles [23]. There is a considerable amount of literature on implanting planar microelectrodes in the microchannel to generate a non-uniform electric field in order to create DEP force [24–26]. The main downside of the planar electrode is the restriction of electric fields to the vicinity of the electrodes, while in three-dimensional electrodes electric field spread through the cross section of the channel. These kinds of electrodes are designed along the sidewall of the device. Therefore, DEP affected area is increased. In [27], the authors presented mixing silver powders with PDMS to conveniently manufacture three-dimensional electrodes for separation of 10 mm and 15 mm particles. Moreover, Botao zho and co-workers [28] investigated liquid metal electrode for red blood cells stretching manipulation and a thin insulating membrane was utilized to separate the main channel from liquid fluid electrode channels. Alternatively, 3D copper electrodes fabricated along the channel sidewall separate yeast cells and white blood cells [29]. Embedding insulator obstacles inside the channel which are fabricated by the same material as a channel inside the microfluidic devices are other approaches to increase the non-uniformity of the electric field. Some researchers utilizing circular obstacles and DC-DEP to separate micro and nanoparticles [30]. While others fabricated sawtooth obstacles in their separation device to investigate the separation mechanism in detail [31].

In this work, we propose four different continuous LOC separation DEP based devices with the combination of obstacles and sidewall gold electrodes. With the purpose of increasing the contact between the particles (RBCs and MDA-MB231 cells) and the electrodes, the inlet divided into two main channels. Numerical simulations are carried out to compare the electric field gradient and velocity flow of the devices. The resultant forces on the particle can be determined by using the solutions of the flow and the electrical field. Additionally, we survey not only the appropriate voltage for having better separation performance to eliminate joule heating effect but also comparing drag and DEP force in the different regions of the chosen layout which have the stronger non-uniform electric fields.

2 Theory

To obtain the motion of the particles in the microfluidic channel, it is critical to investigate the hydrodynamic, DEP and Drag forces. Hydrodynamic force, generated by hydrodynamic flow, is in the same direction of the flow. In Fig. 1, the drag force balances the difference between DEP and hydrodynamic force.

The drag force is created by distributed fluid velocity applies to the spherical particle suspended in the medium governs by stokes' law [32].

$$F_{\text{Drag}} = 6\pi r_{\text{ext}}\eta(\vec{u} - \vec{u}_{\text{p}}) \tag{1}$$

where r_{ext} is the external radius of the particle, η is the viscosity of the medium, u and u_{p} are velocity and velocity of the particle, respectively. The drag force acting on the particles is proportional to the flow velocity. Spherical particles and conductive medium are polarized owing to the exerted electric field. Thus, the interaction of these particles and the electric field gradient could generate DEP force is given by [33].

$$F_{\text{DEP}} = 2\pi r_{\text{ext}}^3 \varepsilon_0 \varepsilon_{\text{m}} \text{Re}[CM(f)]\nabla\left|\vec{E}\right|^2 \tag{2}$$

where E is the electric field, ε_0 and ε_{m} refer to the vacuum permittivity and permittivity of the medium. From Eq. (2), DEP force magnitude is proportional to the gradient of the field magnitude squared and the cube of particle diameter. Hence, particles of different size experience diverse separation distance. Therefore, according to Newton's second law, trajectory of the particles is calculated by obtaining the exerted forces to the particles.

$$\sum \vec{F} = F_{\text{DEP}} + F_{\text{Drag}} = m_{\text{p}}\frac{\text{d}\vec{u}_{\text{p}}}{\text{d}t^2} \tag{3}$$

where m_{p} and is the particle mass in the above equation. We can express the accurate movement of the particles in the main channel by Replacing Eq. (1) (the drag force) and Eq. (2) (DEP force) into Newton's second law
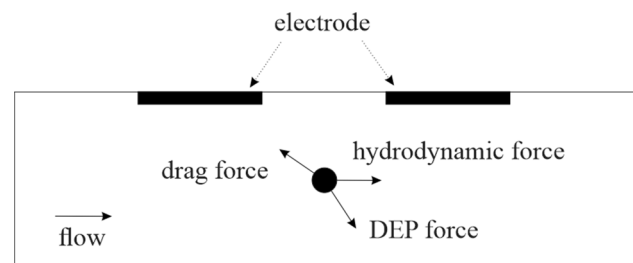

Fig. 1 Schematic illustration of forces acting on the particle

$$2\pi r_{ext}^3 \varepsilon_0 \varepsilon_m \text{Re}[CM(f)]\nabla\left|\vec{E}\right|^2 + 6\pi r_{ext}\eta(\vec{u} - \vec{u}_p) = m_p\frac{d\vec{u}_p}{dt^2}$$
(4)

Re[CM(f)] represents the real part of the Clausius–Mossotti or polarization factor [34], defined as

$$CM(f) = \frac{\varepsilon_p^* - \varepsilon_m^*}{\varepsilon_p^* + 2\varepsilon_m^*}$$
(5)

$$\varepsilon_i^* = \varepsilon_i \varepsilon_0 - j\frac{\sigma_i}{\omega}$$
(6)

where ε_i^* is the complex permittivity, ε_p^* and ε_m^* are the complex permittivities of the particle and medium. The complex permittivity of the dielectric materials depends on their respective conductivities and permittivities. The angular frequency is $\omega = 2\pi f$. The simplest approach to model biological particles is the single-shell model (Fig. 2). In this method, a thin membrane surrounds the cytoplasm. When calculating the DEP fore, equivalent effective complex permittivity is replaced by ε_p in CM factor and expressed as

$$\varepsilon_{eq}^* = \varepsilon_{cm}^* \frac{\left(\frac{r_{ext}}{r_{ext}-th_{cm}}\right)^3 + 2\left(\frac{\varepsilon_{cp}^* - \varepsilon_{cm}^*}{\varepsilon_{cp}^* + 2\varepsilon_{cm}^*}\right)}{\left(\frac{r_{ext}}{r_{ext}-th_{cm}}\right)^3 - \left(\frac{\varepsilon_{cp}^* - \varepsilon_{cm}^*}{\varepsilon_{cp}^* + 2\varepsilon_{cm}^*}\right)}$$
(7)

where th_{cm} is the thickness of the cell membrane, ε_{cp}^* is the complex permittivity of the cytoplasm and ε_{cm}^* is the complex permittivity of the membrane. The value of Re[CM(f)] varies between −0.5 and 1 and represents the sign of the DEP force. In the cases where Re[CM(f)] is positive, the positive DEP forces (pDEP) attract the particles to the high electric field strength. However, in the negative values of Re[CM(f)], the negative DEP force (nDEP) repel particles away from the high electric field regions. Figure 3 represents the real part of the CM factor as a function of electric field frequency ranging from 100 Hz to 10 GHZ and calculated in MATLAB for RBCs and MDA-MB231 cells suspended in the conductive liquid. Two crossover frequencies
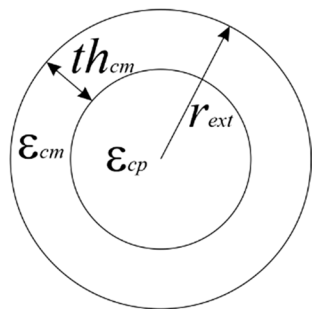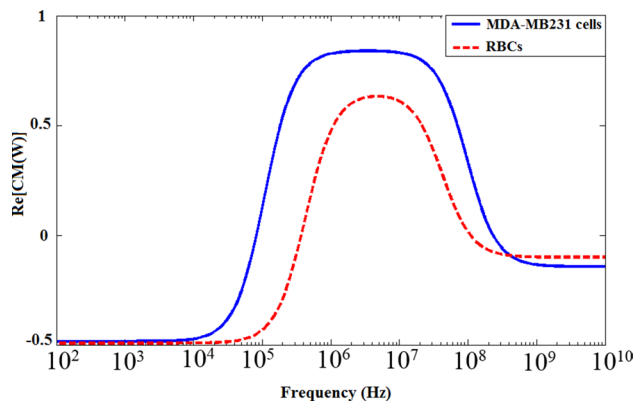

Fig. 3 The real part of the CM factor as a function of frequency for RBC and MDA-MB231

(the point where nDEP switch to the pDEP and vice versa) exist for two-layer particles. CTCs and RBCs had distinct CM factor and also had a unique first crossover frequency with the value of 83 kHz and 367 kHz, respectively. At this frequency, RBCs and cancerous cells experience zero DEP force. The properties of the cells and medium are demonstrated in Table 1 [35, 36]. The table includes the external radius of the particle (r_{ext}), the thickness of the membrane (th_{cm}), the conductivity of the cytoplasm (σ_{cp}) and membrane (σ_{cm}).

In order to compute the performance of the separation device, separation efficiency and separation purity are described. Separation efficiency is defined by counting the number of specific cancerous cells in the outlet over the total number of cancerous cells injected to the device. Furthermore, separation purity is defined as the number of specific cells in the outlet to the total number of target cells in that outlet [37].

$$Efficiency = \frac{Number\ of\ specific\ cell\ types\ (outlet)}{Number\ of\ specific\ cell\ types\ (inlet)}$$
(8)

$$Purity = \frac{Number\ of\ specific\ cell\ types\ (outlet)}{Number\ of\ total\ cells\ (outlet)}$$
(9)

3 Materials and methods

3.1 Device geometry

Schematics of the proposed separation devices are displayed in Fig. 4. Microchannels consist of two different main channels with sidewall electrodes. The length of each main channel is 4200 μm. The presented microseparators have four branches consisting of two inlets (A, B) and two outlets (C,

Fig. 2 Schematic illustration of single-shell particle

Table 1 Physical–chemical properties of RBCs and MDA-MB231

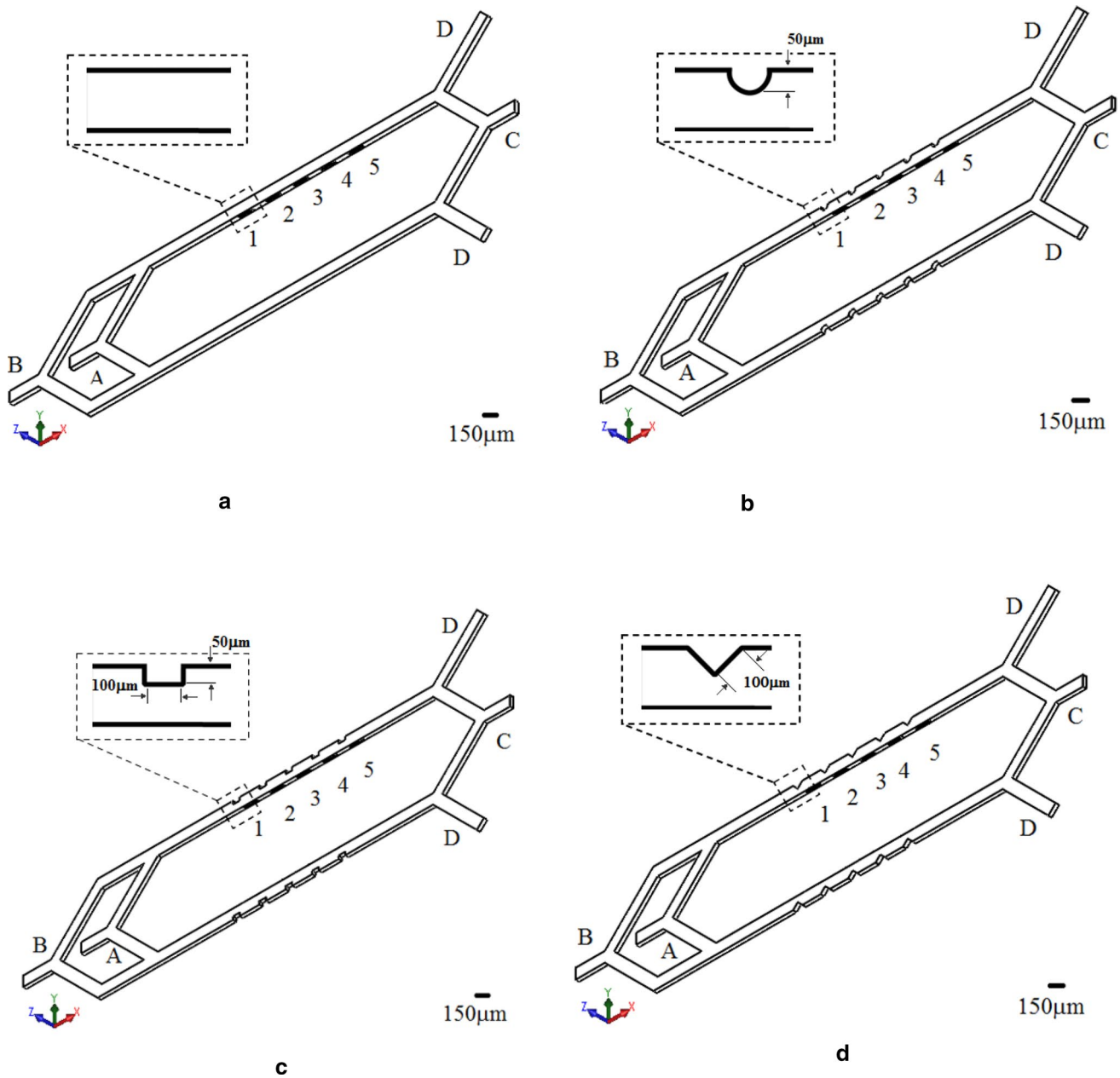| Cell type	r_{ext} (μm)	th_{cm} (nm)	σ_{cm} (μS/m)	σ_{cp} (S/m)	ε_{cp}	ε_{cm}
MDA-MB-231	9	7	0.9	1	50	12.5
RBC	3.2	4.5	0.8	0.4	212	5

m meter, *S* simens

Fig. 4 Proposed microchannels for separation of CTCs and RBCs **a** without obstacles, with **b** circular, **c** rectangular and **d** triangular obstacles and five sidewall electrodes

D). Inlet A is for random injection of the sample, while the guide flow is introduced from another inlet. CTCs and RBCs are collected regardless of the size of the particles from outlet D and C, respectively. The width of the main channels and all branches is 150 μm. The depth is uniform in the entire device with the value of 50 μm. There are 5 electrodes connected to the AC voltage to produce non-uniform electric fields. The electrodes located in the sidewall of the main

channel. The gaps between the electrodes and the width of the electrodes are set to 200 µm. Four different separation microfluidic devices are designed to investigate the performance. Figure 4a demonstrates the channel without any obstacles, whereas Fig. 4b–d show utilizing rectangular, triangular and circular obstacles on the opposite sidewall of the electrodes, respectively. Detailed dimensions of the structures are shown in this figure. Obstacles are embedded both to push the particle toward the electrodes and increase the non-uniformity of the electric fields to improve the separation. The mixture of MDA-MB231 breast cancer cells line and RBCs transported from the inlet A and divided into two main channels to increase the volume of the particles which experienced DEP force. Then, the particles were confined into the region near the electrodes by focusing the flow introduce from branch B. Stronger DEP force acted on bigger particles and transported to the outlet D. However, the smaller particles flowed into branch C.

3.2 Numerical simulation

The finite element method (FEM) software (COMSOL Multiphysics 5.5) was performed to simulate the separation performance of the proposed channel. The simulation is implemented by utilizing the computer with 4 GB RAM and Intel Core i5 2.30 GHz CPU. It was taken about 15 min to complete the simulation. The AC-DC module and the laminar flow module and particle tracking module were employed to evaluate the procedure. In a microfluidic channel with a low Reynolds number, the distribution of the flow field was solved by the laminar flow model and using incompressible Navier–stokes equations.

$$\rho \nabla \cdot \vec{u} = 0 \tag{10}$$

$$\rho(\vec{u} \cdot \nabla)\vec{u} + \rho \frac{\delta \vec{u}}{\delta t} = \nabla \cdot [-P\vec{I} + \mu(\nabla \vec{u} + (\nabla \vec{u})^T)] + \vec{F} \tag{11}$$

In Eq. (11), ρ is the density of the fluid, u is velocity, t is the time, P is the pressure, µ is the fluid viscosity, F is the body force and T is the transpose of a matrix. The pressure of the outlet is set to zero. AC-DC module was used to compute the distribution of the electric field in the device by using the Laplace equation.

$$\nabla \cdot \vec{J} = 0 \tag{12}$$

$$\vec{J} = \sigma \vec{E} + \vec{J}_e \tag{13}$$

$$\vec{E} = -\nabla \vec{V} \tag{14}$$

where J, E, σ and V are current density, electric field, electrical conductivity and voltage, respectively. Electrodes

have constant potential and the inlets, outlets and walls have insulated boundary conditions. The pressure at inlets and outlets was set to zero. The flow rates in branch A and branch B were set to 134[µm/s] and 800[µm/s], respectively. The boundary condition for the wall was prescribed as non-slip. This condition is assumed the existence of the interaction between the fluid and solid surface (wall). The particles were randomly released from A inlet, while the conductivity, the permittivity, the dynamic viscosity and density of the medium were 55[mS/m], 80, 1e-3[Pa×s] and 1000[kg/m³], respectively. The amplitude and frequency of sinusoidal voltage assigned to odd electrodes (counted from left) were 4 to 6 V, 10 kHz and others were −4 to −6 V, 10 kHz. Particle trajectory in the separation devices can predict by particle trajectory tracking module by coupling the flow field and electric field in the channel.

To reinforce the accuracy of the separation devices, finding the proper size and number of the meshes is crucial. Therefore, the distribution of the electric field in the center of the channel (Fig. 5) for all presented devices is investigated by different triangular mesh sizes. In all graphs normal, fine and finer mesh sizes are illustrated by solid blue and solid orange lines and dashed red line, respectively. Electrodes are connected to the 6 V and −6 V AC voltage with the frequency of 10 kHz. It can be seen from Fig. 5 that different mesh size has little impact on the electric field distribution. Hence, a triangular fine mesh size is chosen for computation (Fig. 6). The total number of grids are 26,510, 29,008, 26,936 and 26,756 for presented devices. Obviously, the number of grids is used near the obstacles and electrodes are higher than other parts to improve the calculation.

4 Results and discussion

For comparison purpose, numerical simulation was performed by the aforementioned numerical model to acquire the influence of different obstacle shapes in presented channels with the same voltage and flow velocity. Hence, the distribution of the electric field as well as velocity was investigated to obtain the appropriate design. Obviously, RBCs and MDA-MB231cells experienced nDEP at 10 kHz and moved toward the negative direction of the gradient fields. A comparison of the y-component of DEP and drag force and particle trajectory of the cells for the chosen design layout was studied. These four geometries had symmetric structures; therefore, the upper part of the devices was investigated.

The distribution of the velocity field as well as the electric field force is shown in Figs. 7 and 8, respectively. Furthermore, the influence of the obstacles on the MDA-MB231 cell in the separation channel was investigated. Y-component of the velocity field is the key factor of the separation studied for all the proposed channel. According to Fig. 7a,
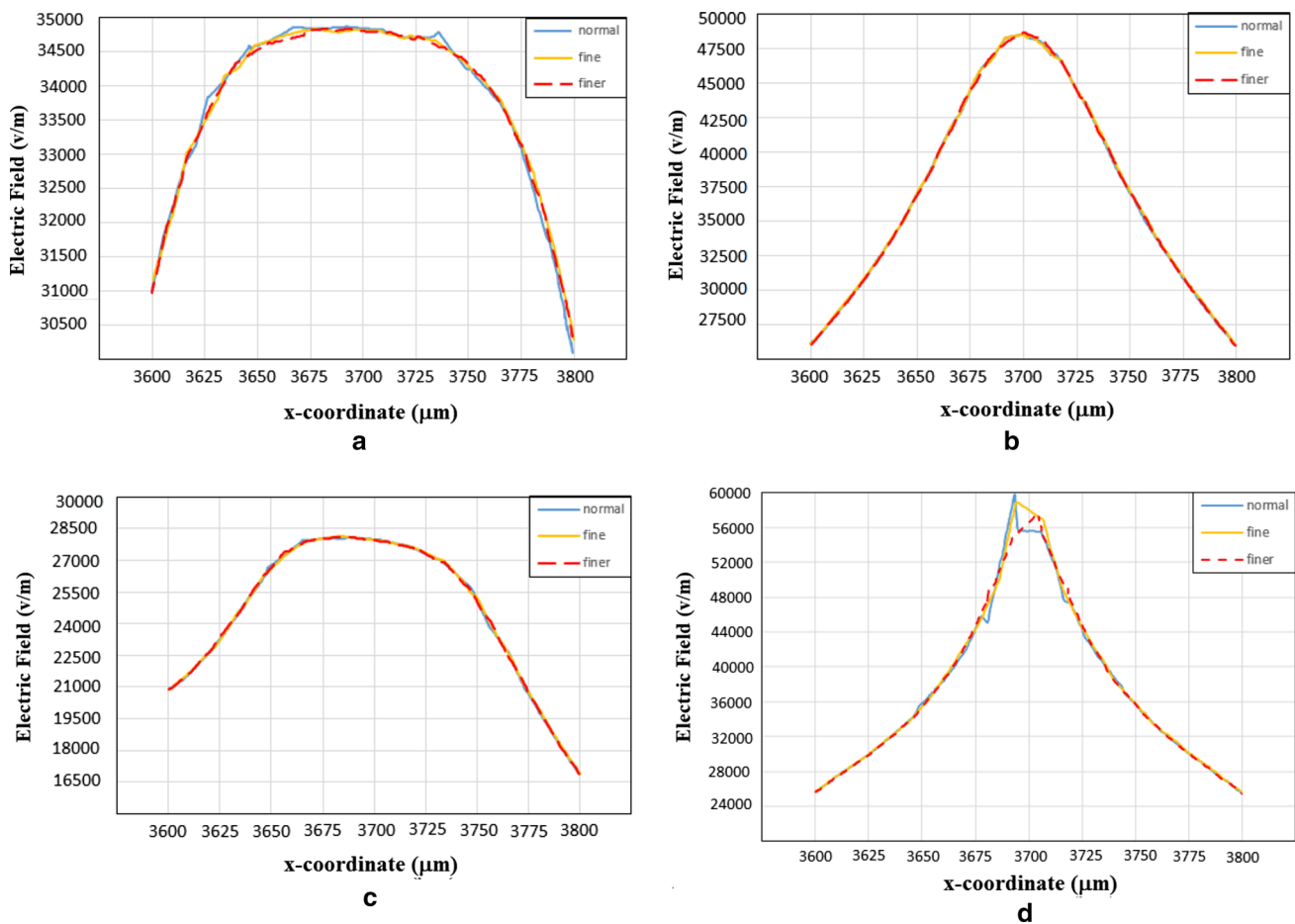
Fig. 5 Distribution of electric field between fourth and fifth electrodes in: **a** microchannel without obstacles and main channel with **b** circular, **c** square and **d** triangular obstacles

the velocity distribution is uniform inside the channel, thus particle could only separate because of DEP force and the drag force was neglected. However, in Fig. 7b–d, cells experience the various magnitude of the velocity in the different vertical distances. A stronger velocity field was observed in the center of the channel and between the obstacles and the opposite wall, although the magnitude of the velocity decreased at the center of the channel between the obstacles. Both DEP and drag force, therefore, were contributed to the separation of bigger and smaller particles. Figure 8 shows both contour of the electric fields and DEP force demonstrated by arrows. High electric fields were observed in the edge of the electrodes and contraction region near the obstacles (Fig. 8b–d). DEP forces acting on MDA-MB231 cells and RBCs are represented by blue and red arrows, respectively. Microchannel with obstacles had a stronger magnitude of the field in both edges of the electrodes and the vicinity of the obstacles indicated that CTC cells experience stronger nDEP force. These tests revealed that obstacles not only increase the electric field non-uniformity beside them but also push the cells to flow near the electrodes.

Consequently, devices with rectangular obstacles had the best separation performance (this design has a bigger path below the obstacles) among the presented designs and deflected cancerous cells to branch D.

It is crucial to note that, cells inside the channel experienced several regions where either one of the forces was dominated or they had equal amplitude. According to Eq. (1), y-component of the drag force is not only proportional to the velocity but also proportional to the external radius of the cells. Hence, as observed in Fig. 5d, five maximum amplitude of the drag force was observed (Fig. 9) due to the 5 maximum velocity regions inside the channel near the obstacles. As discussed previously, it is important to consider the gradient of the electric fields and external radius of the cells to investigate the y-component of DEP force (Fig. 9) inside the main channel. MDA-MB231 experienced stronger nDEP in magnitude than RBCs because of a bigger radius and different dielectric properties. As observed before, the first obstacles cells were subjected to equal DEP and drag force. As anticipated, in this region, CTCs cells did not separate from RBCs and pass the unit. Due to the

Fig. 6 Mesh map of: **a** simple microseparators and microchannel with **b** circular, **c** square and **d** triangular obstacles. orange lines represented the electrodes which located between the obstacles
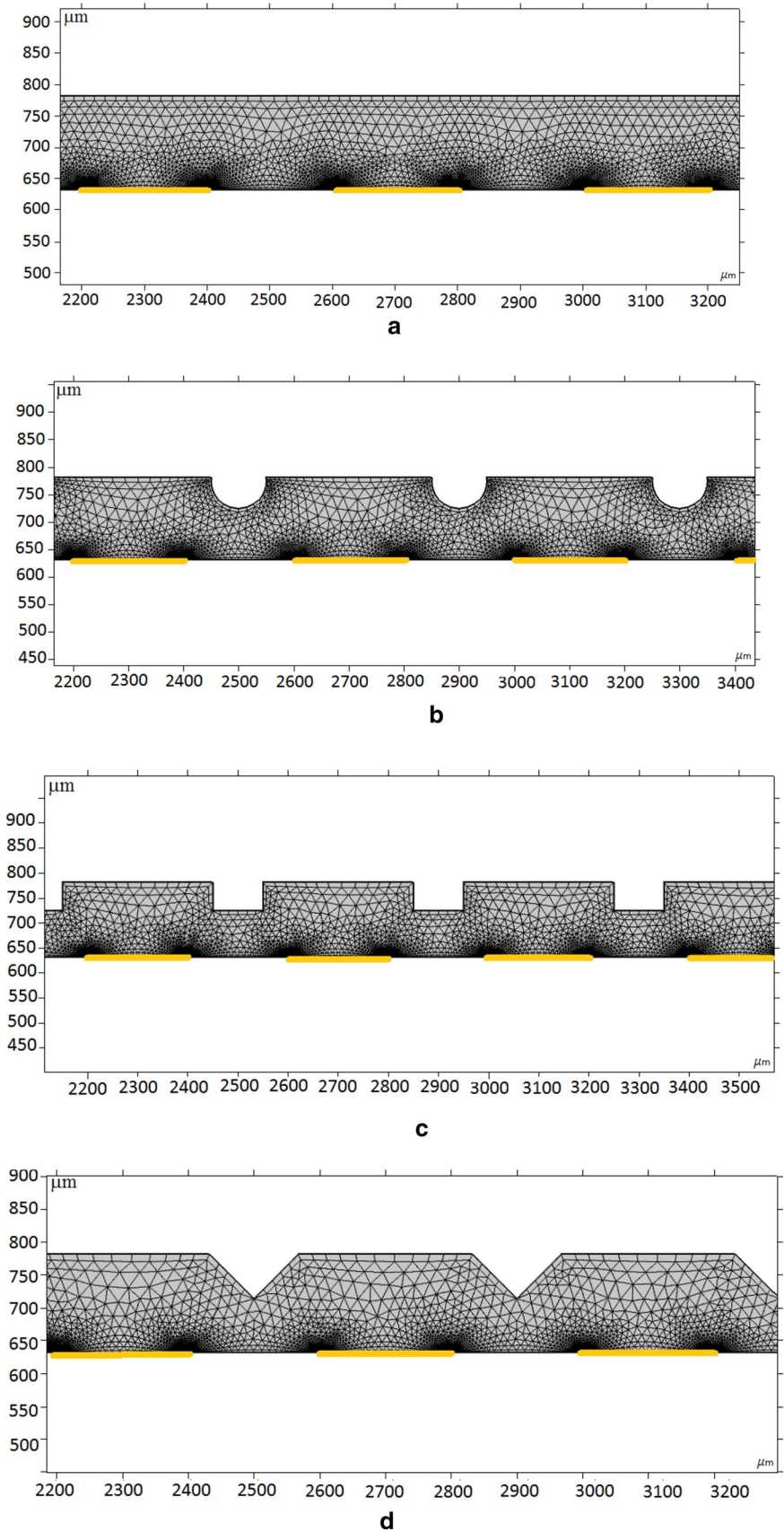
Fig. 7 Velocity distribution inside the microdevices: **a** without obstacles, with **c** circular, **b** square and **d** triangular obstacles. Higher velocity is shown the contraction areas under the obstacles
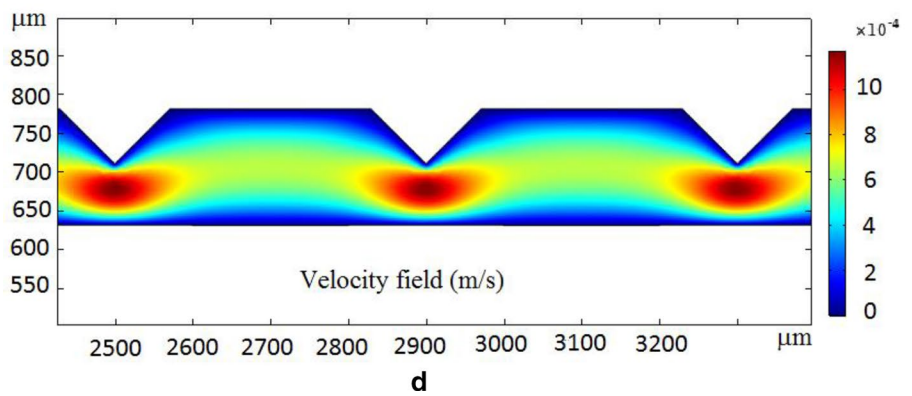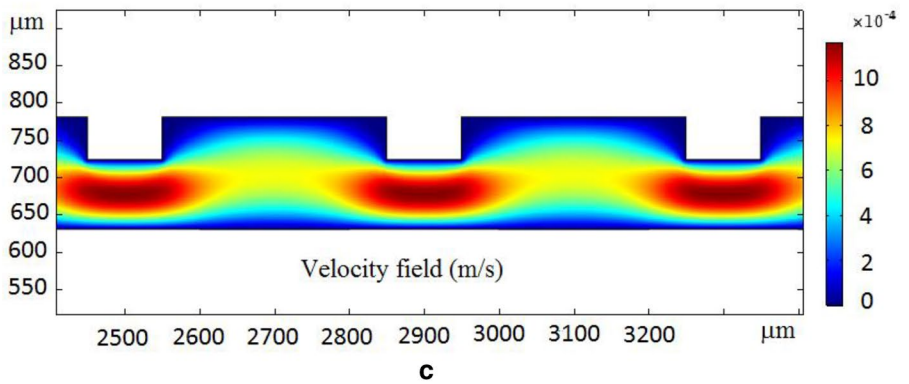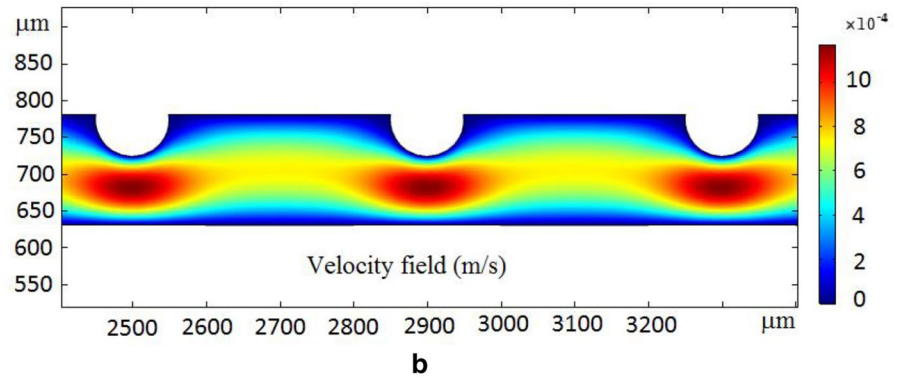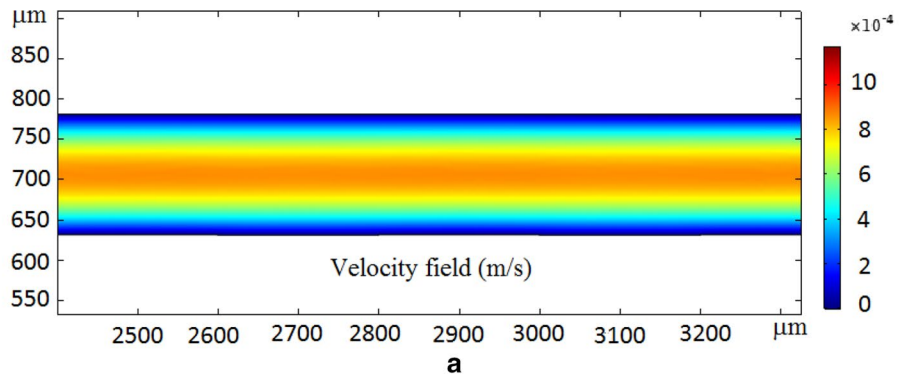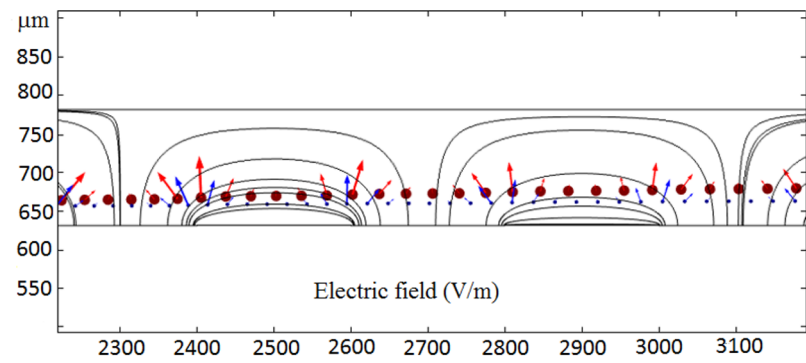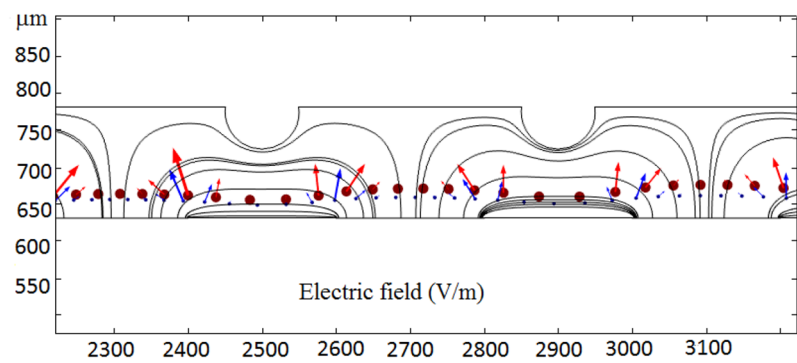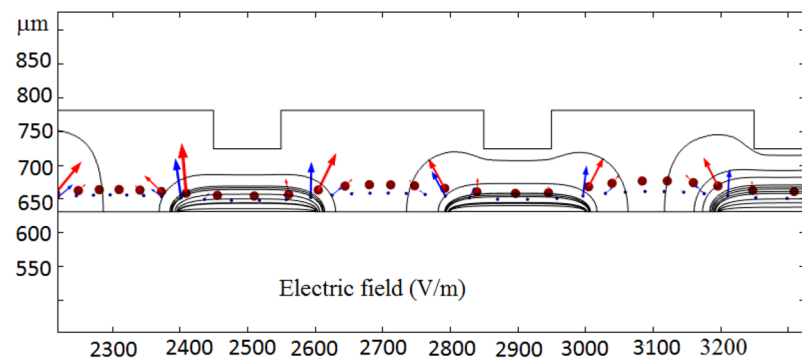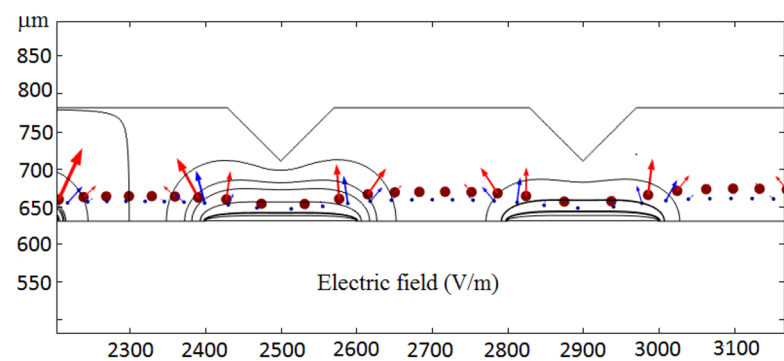
Fig. 8 The contour of the non-uniform electric fields and the arrows represent the DEP force. **a** Simple channel and microseparators with **b** circular, **c** square and **d** triangular obstacles. Owing to the higher electric fields near the obstacles, the arrows of the DEP force are bigger than other parts
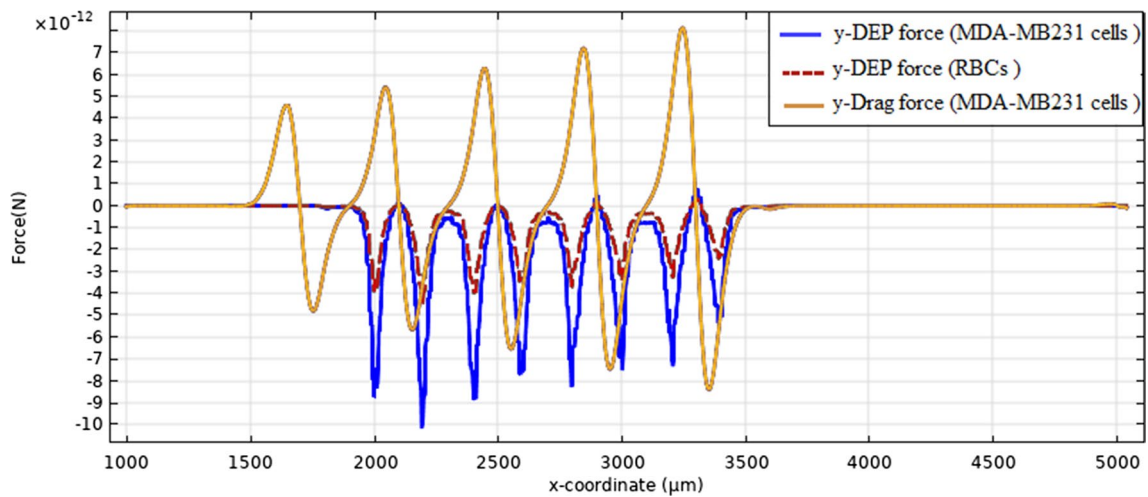
Fig. 9 The magnitude of DEP force acting on RBCs and MDA-MB231 cells and Drag force acting on MDA-MB231along the y-axis

high velocity in the contraction region near the obstacles, magnitude of the DEP force was smaller than drag force ($x = 1700$ μm). In this region, the DEP force was neglected and the particles deflect owing to the drag force. In the third region which was near the first edge of the electrode ($x = 2000$ μm), DEP force was dominated and the particles separate as a result of the y-component of DEP force. In the region where particles flowed between the two edges, DEP force was negligible. In the next edge of the electrodes, drag force was smaller than DEP force. In this case, cells were repelled from the high gradient electric fields. This process was similar in the other parts of the channels until cancerous cells and RBCs were deflected to the D and C branches, respectively.

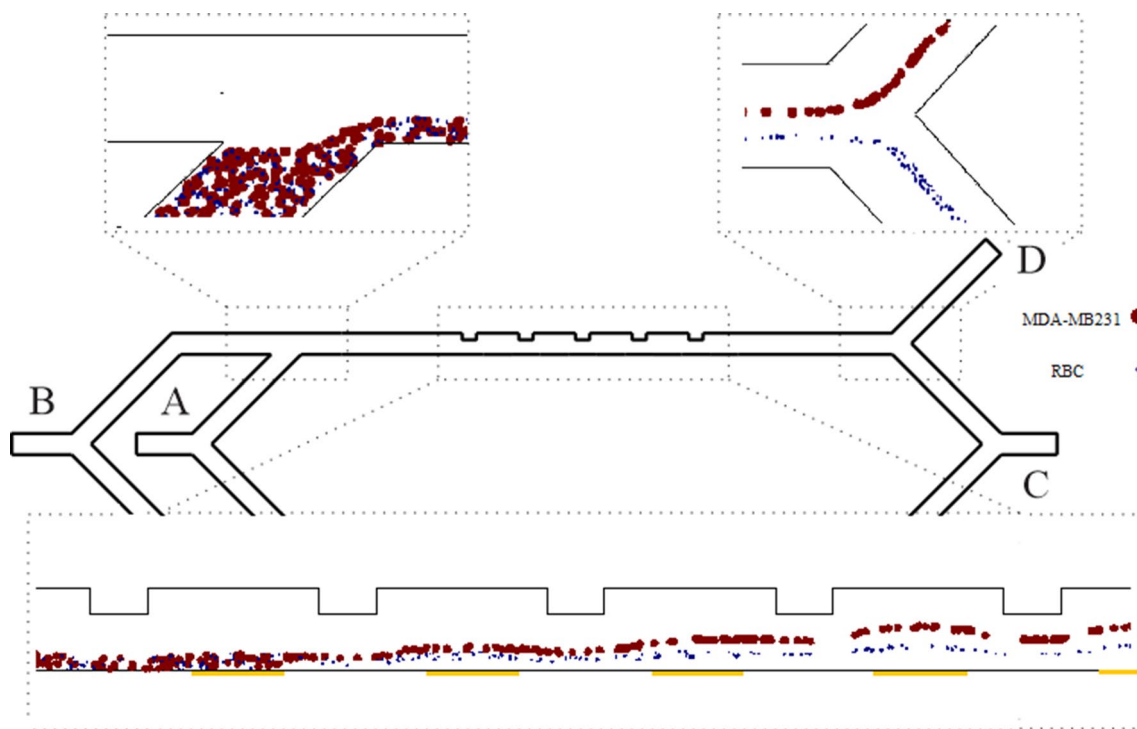We also carried out the study on particle trajectory (Fig. 10) to better understand the separation process of the

Fig. 10 Particle trajectory of RBCs and CTCs inside the channel with rectangular obstacles

particles owing to the DEP and drag force. Before the first obstacles buffer fluid focused the cells along the sidewall. As observed, cells started to separate from the back edges of the first electrodes (yellow line in Fig. 10), and each particle was deflected to the specific outlet after the last electrodes. As expected, second, third and fourth obstacles pushed the particles toward the electrodes and repelling effects observed near the electrodes.

The applied voltage to the sidewall electrodes is a significant parameter that should be regarded for the optimization of the separation efficiency. Different voltages were discussed to find the optimum voltage. Because of changing the electric field gradient, altering the voltage could affect the movement of the particles and deviate them from the primary streamlines. As shown in Fig. 11a–c, when the potential of the odd electrodes and others were set to 4 V and −4 V, respectively, the electric fields were not sufficient to separate effectively and particles came out from the outlet C. By increasing the voltage to 5 V and −5 V (Fig. 11b), some of the MDA-MB231 cells experienced sufficient electric field and subjected to the DEP force, whereas others deflect to outlet C as well as RBCs. Increasing the voltage

Fig. 11 Numerical simulation of particles trajectory of RBCs and CTCs for various voltages **a** 4 V and −4 V, **b** 5 V and −5 V, **c** 6 V and −6 V
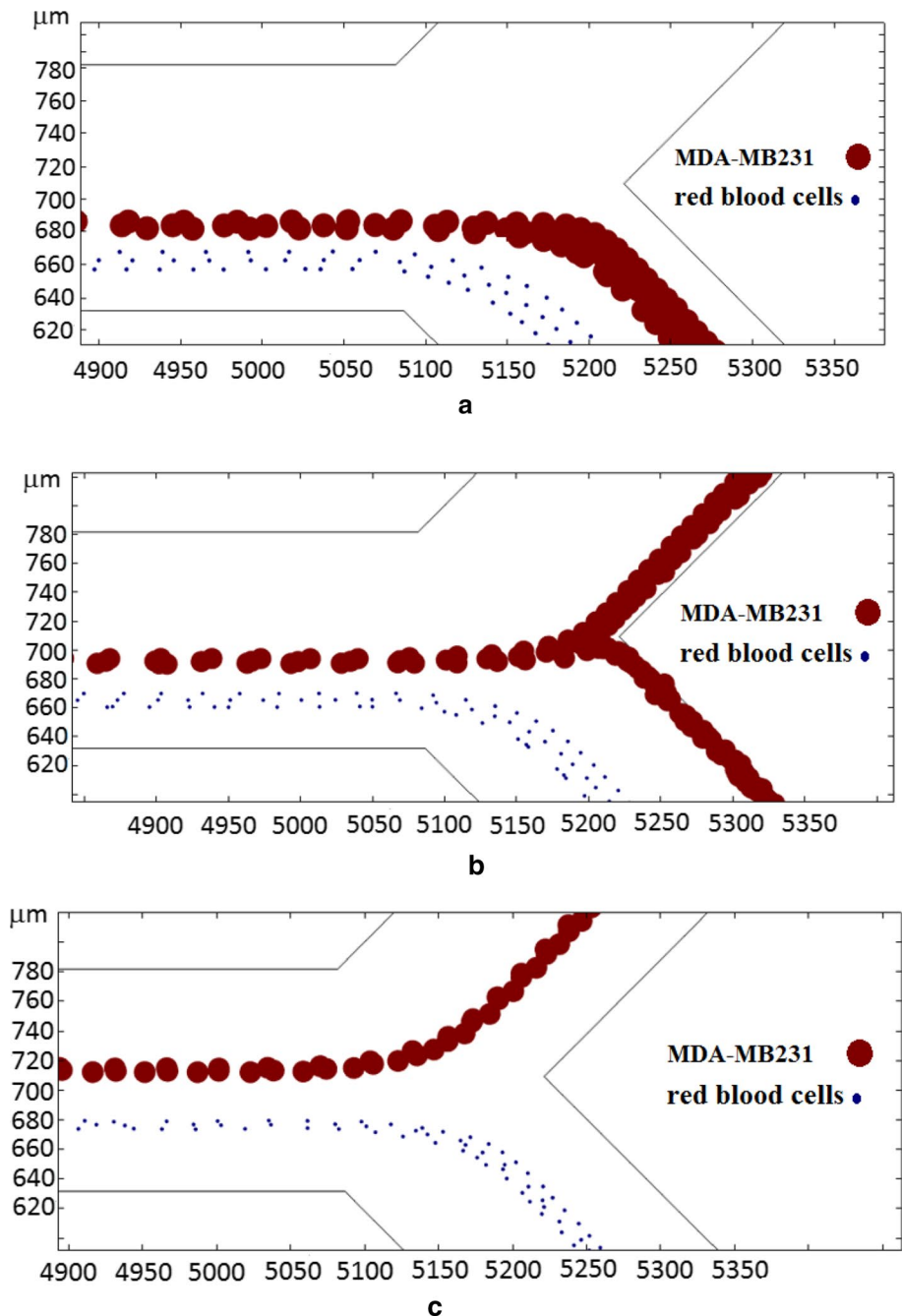
could generate a higher gradient of the electric field and producing uniform DEP force along the height of the channel. As expressed in Eq. (2), the cubic power of the particle size is proportional to the DEP force. When the value of the voltage further increased to 6 V and −6 V, owing to the abovementioned reason MDA-MB231 cells reached farther lateral displacement than RBCs cells. Consequently, bigger and smaller cells were directed toward the outlet D and outlet C, respectively.

Despite the device in [27] which was time-consuming to completely separate the particles, the microfluidic device presented in this study could easily separate a large number of CTCs and RBCs because of using two main channels. The separation efficiency and purity of the particles in the different voltages are observed in Fig. 12a and b. Applying 6 V to the (1,3,5) electrodes and −6 V to the others had the 100% separation efficiency and 100% separation purity in D branch for CTCs which had better performance. However, the separation purity and efficiency of the MDA-MB231 cells decreased by reducing the applied voltages in outlet D. 46% of cancerous

cells was deflected to the outlet D owing to insufficient electric fields by decreasing from 6 V and −6 V to 5 V and −5 V.

Electric fields led to generating Joule heating and increasing the temperature of the electrolyte. Increasing the temperature of the fluid could change the properties of the fluid and arose the electrochemical reactions inside the channel [38]. In the case of using obstacles and dividing the inlets into the two main channels, the lower potential was applied to the electrodes. Thus, the lower amplitude of the applied voltage minimized the destructive effects of Joule heating. It can be found that particles could separate without adverse effects such as joule heating while the value of voltage is equal to 6 V and −6 V for (1,3,5) electrodes and (2,4). The maximum temperature (ΔT) raises in the microfluidic device is calculated by [39]

$$\Delta T = \frac{\sigma_{\mathrm{m}} V^2}{16 k_{\mathrm{m}}}$$

Fig. 12 Separation efficiency and separation purity in **a** outlet D and **b** of the device with rectangular obstacles for RBCs and MDA-MB231
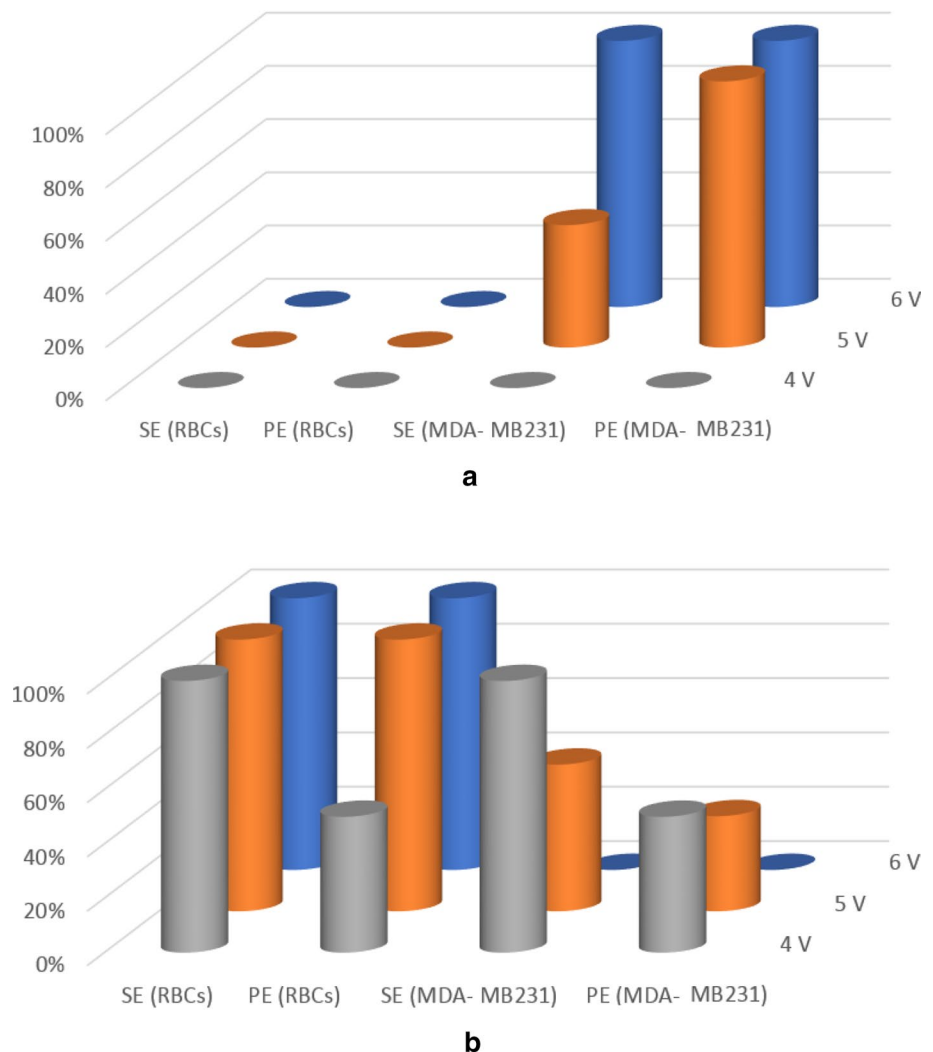
where V is the applied voltage, $V = \sqrt{2} \times V_{rms}$, $k_m = 0.6$ J m^{-1} s^{-1} k^{-1} is the thermal conductivity and σ_m is the electrical conductivity of the liquid medium. In this study, $\Delta T = 0.2$ °C is calculated. Increasing the number of electrodes could increase the area which experienced DEP force. Accordingly, it is possible to decrease the magnitude of the voltage in separation devices by more electrodes. 21.25 s after introducing the first cells into branch A, particles exited from the outlets. Fabrication of two main channels halved the performance time in comparison to the one channel devices.

5 Conclusion

Different platforms have been designed for continuous separation of MDA-MB231 cells from red blood cells using a label-free and negative AC dielectrophoresis force at 10 kHz. Separation devices take the advantages of sidewall electrodes along with obstacles inside the channels to generate non-uniform electric fields over entire channels. A combination of drag and DEP force deflect cells to specific outlets. Designing two main channels not only reduced the separation times but also increased the regions experienced dielectrophoresis force and facilitate the process. Series of numerical simulations were performed to survey the distribution of electric fields and velocity flow. Meanwhile, a microchannel with the best separation performance was chosen and several different voltages were applied to investigate the Joule heating effect. Further, separation efficiency and purity were calculated for these different voltages.

It is worth to note that the combination of DEP and passive methods will be analyzed in our future work. These two methods are able to increase the efficiency of the device and to decrease the separation time. The presented platform can pave the way for a fast diagnosis of CTCs from normal blood cells.

References

1. Zhang J, Yang S, Chen C, Hartman JH, Huang P-H, Wang L, Tian Z, Zhang P, Faulkenberry D, Meyer JN (2019) Surface acoustic waves enable rotational manipulation of *Caenorhabditis elegans*. Lab Chip 19(6):984–992
2. Medoro G, Guerrieri R, Manaresi N, Nastruzzi C, Gambari R (2007) Lab on a chip for live-cell manipulation. IEEE Des Test Comput 24(1):26–36
3. Valijam S, Veladi H, Baghban H, Zargari S (2018) High-efficiency passive micromixer using three-dimensional printed molds. J Micro/Nanolithogr MEMS MOEMS 17(2):025002
4. Chuang C-H, Wu H-P, Huang Y-W, Chen C-H, Lee D-H, Wu T-F (2016) A rapid and sensitive impedance-based immunosensor utilizing dielectrophoretic manipulations of polyaniline modified nanoprobes. IEEE Sens J 16(11):4166–4173
5. Ho C-T, Lin R-Z, Chang W-Y, Chang H-Y, Liu C-H (2006) Rapid heterogeneous liver-cell on-chip patterning via the enhanced field-induced dielectrophoresis trap. Lab Chip 6(6):724–734
6. Ozkumur E, Shah AM, Ciciliano JC, Emmink BL, Miyamoto DT, Brachtel E, Yu M, Chen P-I, Morgan B, Trautwein J (2013) Inertial focusing for tumor antigen–dependent and–independent sorting of rare circulating tumor cells. Sci Transl Med 5(179):179ra147
7. Zhang C, Yu D, Xing X (2020) High velocity dielectrophoretic cell separation using continuously extended sidewall electrode featuring undercut profile. In: 2020 IEEE 33rd international conference on micro electro mechanical systems (MEMS). IEEE, pp 1044–1047
8. Plaks V, Koopman CD, Werb Z (2013) Circulating tumor cells. Science 341(6151):1186–1188
9. Kerr BA, Miocinovic R, Smith AK, West XZ, Watts KE, Alzayed AW, Klink JC, Mir MC, Sturey T, Hansel DE (2015) CD117+ cells in the circulation are predictive of advanced prostate cancer. Oncotarget 6(3):1889
10. Lee J-H, Lee S-K, Kim J-H, Park J-H (2019) Separation of particles with bacterial size range using the control of sheath flow ratio in spiral microfluidic channel. Sens Actuators A 286:211–219
11. Uskoković V, Tang S, Wu VM (2019) Targeted magnetic separation of biomolecules and cells using earthicle-based ferrofluids. Nanoscale 11(23):11236–11253
12. Wu M, Huang PH, Zhang R, Mao Z, Chen C, Kemeny G, Li P, Lee AV, Gyanchandani R, Armstrong AJ (2018) Circulating tumor cell phenotyping via high-throughput acoustic separation. Small 14(32):1801131
13. Khan SA, Chang C-M, Zaidi Z, Shin W, Shi Y, Bowden AKE, Solgaard O (2016) Metal-insulator-metal waveguides for particle trapping and separation. Lab Chip 16(12):2302–2308
14. Aghaamoo M, Aghilinejad A, Chen X, Xu J (2019) On the design of deterministic dielectrophoresis for continuous separation of circulating tumor cells from peripheral blood cells. Electrophoresis 40(10):1486–1493
15. He C, Chen S, Zhao J, Tian J, Zhao S (2020) Ultrasensitive detection of microRNA-21 based on electrophoresis assisted cascade chemiluminescence signal amplification for the identification of cancer cells. Talanta 209:120505
16. Tada S, Hayashi M, Eguchi M, Tsukamoto A (2017) High-throughput separation of cells by dielectrophoresis enhanced with 3D gradient AC electric field. Biomicrofluidics 11(6):064110
17. Froberg J, Jayasooriya V, You S, Nawarathna D, Choi Y (2017) Quantitative measurements of dielectrophoresis in a nanoscale electrode array with an atomic force microscopy. Appl Phys Lett 110(20):203701
18. Gonzalez CF, Remcho VT (2005) Harnessing dielectric forces for separations of cells, fine particles and macromolecules. J Chromatogr A 1079(1–2):59–68
19. Zhao K, Li D (2017) Continuous separation of nanoparticles by type via localized DC-dielectrophoresis using asymmetric nano-orifice in pressure-driven flow. Sens Actuators B Chem 250:274–284
20. Jiang T, Ren Y, Liu W, Tang D, Tao Y, Xue R, Jiang H (2018) Dielectrophoretic separation with a floating-electrode array embedded in microfabricated fluidic networks. Phys Fluids 30(11):112003
21. Zhang Y, Chen X (2020) Blood cells separation microfluidic chip based on dielectrophoretic force. J Braz Soc Mech Sci Eng 42:1–11
22. Cetin B, Li D (2008) Effect of Joule heating on electrokinetic transport. Electrophoresis 29(5):994–1005
23. Voldman J (2006) Electrical forces for microscale cell manipulation. Annu Rev Biomed Eng 8:425–454
24. Hsiung L-C, Yang C-H, Chiu C-L, Chen C-L, Wang Y, Lee H, Cheng J-Y, Ho M-C, Wo AM (2008) A planar interdigitated ring

electrode array via dielectrophoresis for uniform patterning of cells. Biosens Bioelectron 24(4):869–875

25. Pethig R (2010) Dielectrophoresis: Status of the theory, technology, and applications. Biomicrofluidics 4(2):022811

26. Li H, Bashir R (2002) Dielectrophoretic separation and manipulation of live and heat-treated cells of Listeria on microfabricated devices with interdigitated electrodes. Sens Actuators B Chem 86(2–3):215–221

27. Lewpiriyawong N, Yang C, Lam YC (2010) Continuous sorting and separation of microparticles by size using AC dielectrophoresis in a PDMS microfluidic device with 3-D conducting PDMS composite electrodes. Electrophoresis 31(15):2622–2631

28. Zhu B, Cai Y, Wu Z, Niu F, Yang H (2019) Dielectrophoretic Microfluidic Chip Integrated With Liquid Metal Electrode for Red Blood Cell Stretching Manipulation. IEEE Access 7:152224–152232

29. Çetin B, Kang Y, Wu Z, Li D (2009) Continuous particle separation by size via AC-dielectrophoresis using a lab-on-a-chip device with 3-D electrodes. Electrophoresis 30(5):766–772

30. Chen D, Du H (2010) A microfluidic device for rapid concentration of particles in continuous flow by DC dielectrophoresis. Microfluid Nanofluid 9(2–3):281–291

31. Chen KP, Pacheco JR, Hayes MA, Staton SJ (2009) Insulator-based dielectrophoretic separation of small particles in a sawtooth channel. Electrophoresis 30(9):1441–1448

32. Nguyen N-T, Wereley ST, Shaegh SAM (2019) Fundamentals and applications of microfluidics. Artech House, Boston

33. Prakash S, Yeom J (2014) Nanofluidics and microfluidics: systems and applications. William Andrew, Norwich

34. Çetin B, Li D (2011) Dielectrophoresis in microfluidics technology. Electrophoresis 32(18):2410–2427

35. Sano MB, Henslee EA, Schmelz E, Davalos RV (2011) Contactless dielectrophoretic spectroscopy: examination of the dielectric properties of cells found in blood. Electrophoresis 32(22):3164–3171

36. Zhang Y, Chen X (2020) Dielectrophoretic microfluidic device for separation of red blood cells and platelets: a model-based study. J Braz Soc Mech Sci Eng 42(2):89

37. Büyükkoçak S, Özer MB, Cetin B (2014) Numerical modeling of ultrasonic particle manipulation for microfluidic applications. Microfluid Nanofluid 17(6):1025–1037

38. Oh J, Hart R, Capurro J, Noh HM (2009) Comprehensive analysis of particle motion under non-uniform AC electric fields in a microchannel. Lab Chip 9(1):62–78

39. Ramos A, Morgan H, Green NG, Castellanos A (1998) Ac electrokinetics: a review of forces in microelectrode structures. J Phys D Appl Phys 31(18):2338